Cell Shape Can Mediate the Spatial Organization of the Bacterial Cytoskeleton

Siyuan Wang and Ned S. Wingreen*
Lewis-Sigler Institute for Integrative Genomics and Department of Molecular Biology, Princeton University, Princeton, New Jersey

ABSTRACT The bacterial cytoskeleton guides the synthesis of cell wall and thus regulates cell shape. Because spatial patterning of the bacterial cytoskeleton is critical to the proper control of cell shape, it is important to ask how the cytoskeleton spatially self-organizes in the first place. In this work, we develop a quantitative model to account for the various spatial patterns adopted by bacterial cytoskeletal proteins, especially the orientation and length of cytoskeletal filaments such as FtsZ and MreB in rod-shaped cells. We show that the combined mechanical energy of membrane bending, membrane pinning, and filament bending of a membrane-attached cytoskeletal filament can be sufficient to prescribe orientation, e.g., circumferential for FtsZ or helical for MreB, with the accuracy of orientation increasing with the length of the cytoskeletal filament. Moreover, the mechanical energy can compete with the chemical energy of cytoskeletal polymerization to regulate filament length. Notably, we predict a conformational transition with increasing polymer length from smoothly curved to end-bent polymers. Finally, the mechanical energy also results in a mutual attraction among polymers on the same membrane, which could facilitate tight polymer spacing or bundling. The predictions of the model can be verified through genetic, microscopic, and microfluidic approaches.

INTRODUCTION

The shape of a bacterial cell influences many aspects of its life, including nutrient access, motility, chemotaxis, and resistance to predation (1–4). For most bacteria, shape is determined by a mechanically sturdy cell wall (5), and to construct a properly shaped cell wall, bacteria must spatially coordinate cell-wall synthesis. Recently several cytoskeletal proteins have been shown to be essential for this spatial coordination (6–9), leading to the conclusion that proper localization of the bacterial cytoskeleton is required for proper spatial regulation of cell-wall synthesis. However, up to now the mechanisms responsible for proper localization of bacterial cytoskeletal elements have not been clear.

Bacteria have cytoskeletal homologs of all three of the major eukaryotic cytoskeletal elements (Fig. 1 *A*) (6): FtsZ, a tubulin homolog, localizes into a ring (called the Z-ring) at midcell and guides cell division (10,11); when FtsZ is depleted, rod-shaped bacteria such as *Escherichia coli* grow into long filaments (12). MreB, an actin homolog, forms helical segments in *E. coli*, and is required for rod shape (13,14); when MreB is disassembled or depleted, rod-shaped cells gradually grow into spheres after several doubling times (8,15). CreS (crescentin), an intermediate filament homolog, localizes along the inner curvature of *Caulobacter crescentus*, and is essential for the curved rod morphology of these cells (9,16); when CreS is depleted, curved cells grow straight (9,16). All three of these bacterial cytoskeletal proteins attach to the cytoplasmic side of the cell membrane, either directly (MreB) or indirectly through auxiliary proteins (FtsZ) (6,10,17).

Among the three, FtsZ has been most intensively studied. Cryo-electron microscopy indicates that the Z-ring in vivo consists of short protofilaments of 80–160 nm in length (18). These protofilaments align in an approximately circumferential direction often with a regular ~9-nm spacing (18). In vitro, FtsZ monomers polymerize into filaments in the presence of GTP, and these filaments have a straight or slightly curved morphology with a curvature of ~0.01 nm^{-1} (19,20). FtsZ catalyzes GTP hydrolysis (19), and the resultant GDP-bound polymer adopts a highly curved mini-ring conformation with a 23-nm diameter (19). This conformational transition was proposed to generate a constriction force to facilitate cell division (21). There has been no report on the in vitro conformation of *E. coli* MreB. *Thermotoga maritima* MreB shows a double-filament structure on a lipid membrane surface, and can distort the membrane (17). CreS assembles into filaments in vitro without energy requirements (9), but the shape of the filaments has not been well characterized.

Previous theoretical work on the bacterial cytoskeleton mainly focused on the polymerization kinetics and force generation of FtsZ (22–27). In most of these studies, the cellular orientation of FtsZ was arbitrarily constrained. To understand FtsZ's preference for the circumferential direction, Paez et al. (28) simulated FtsZ polymerization on a fine triangular lattice, and enabled 24 discrete directions. They showed that on a cylindrical surface, FtsZ polymers can self-align in the circumferential direction when the polymers have a spontaneous curvature (28).

Importantly, none of these previous theoretical works addressed the influence of membrane energetics on the localization of the bacterial cytoskeleton. In bacteria such as *E. coli,* the cell membrane is constrained by turgor pressure that pushes the cell membrane outward, and by the

Submitted September 11, 2012, and accepted for publication December 11, 2012.

*Correspondence: wingreen@princeton.edu

Editor: Douglas Robinson.

0006-3495/13/02/0541/12 $2.00

http://dx.doi.org/10.1016/j.bpj.2012.12.027

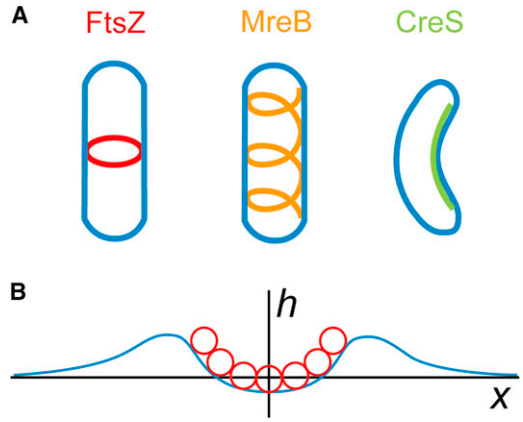

FIGURE 1 Bacterial cytoskeletal polymers. (*A*) Various orientations adopted by bacterial cytoskeleton components. (*B*) Schematic illustration of the polymer-membrane model.

surrounding cell wall that resists membrane expansion (if the cell wall develops a large hole, e.g., due to antibiotic treatment, turgor pressure can cause the cell membrane to bulge out through the hole in the cell wall (29)). The turgor pressure is mainly due to the difference in K^+ concentration across the cell membrane (30,31), with lesser contributions from other cytoplasmic ions and small molecules. Because of the opposing forces of turgor pressure and cell-wall confinement, any deviation from the resulting equilibrium pinned conformation of the membrane is energetically unfavorable (32,33). Moreover, any additional, membrane curvature incurs a further bending energy cost (34,35). On the other hand, membrane-associated cytoskeletal filaments may have their own energetically preferred intrinsic curvatures, which in general will not match the local curvature of the membrane. As a result, when a cytoskeletal polymer interacts with the cell membrane, they will deform each other to minimize total energy. As a corollary, the cytoskeleton will tend to adopt a localization pattern on the membrane that minimizes this total energy.

Some insight into cytoskeletal localization can be drawn directly from the principle of energy minimization. In a rod-shaped cell such as *E. coli*, a cytoskeletal polymer with zero intrinsic curvature would preferentially align with the cell's long axis, as in this way neither the membrane nor the polymer would be deformed. In contrast, a polymer with an intrinsic curvature larger than the cell's circumferential curvature would favor a circumferential orientation (or, alternatively, might localize to the poles). Finally, a polymer with a moderate intrinsic curvature, smaller than the cell's circumferential curvature, would favor a diagonal (helical) orientation. If such a polymer is also intrinsically twisted, the polymer would favor one helical chirality over the other. A similar orientation-selection mechanism, without taking into account the membrane energetics, has been proposed by Andrews and Arkin (36). However, orientation selection is artificially enhanced for a nondeformable membrane as considered in Andrews and Arkin (36), so it is important to determine the precision of polymer orientation selection including realistic membrane mechanics. Membrane-energy considerations may also influence the lengths of cytoskeletal filaments. In particular, short filaments can bind and bend the membrane without causing large deviations from the equilibrium membrane conformation, thus favoring filaments with short length.

These qualitative intuitions demand quantitative validation. For example, because FtsZ forms protofilaments of only ~100 nm in length (18), one may ask how accurately such short fragments can orient circumferentially by energetics alone. Furthermore, without quantitative analysis, it is impossible to predict exactly what conformations cytoskeletal filaments will adopt, what lengths will be preferred, or how multiple filaments will interact with each other through membrane deformation.

In this work, we formulate a simple model that unifies cytoskeletal-polymer and membrane mechanics, and solve for minimum-energy conformations. Using this analytical framework, we predict a novel, to our knowledge, conformational transition of the polymer-membrane system from smoothly curved to end-bent polymers with increasing polymer length. We also quantify polymer length control via membrane energetics, and find that the competition between polymerization energy and mechanical energy can regulate polymer length. We show that membrane-polymer energetics can robustly orient circumferential FtsZ-like polymers, and can accurately prescribe the helical orientation of MreB-like polymers, with longer polymers adopting their preferred orientation with higher accuracy. Moreover, the precise helical orientation of MreB-like polymers is predicted to depend on cell radius, which may be crucial for a feedback mechanism to control cell width. Finally, we show that membrane mechanics leads to mutual attraction among polymers on the same membrane, which may facilitate polymer bundling. We propose experimental means to test the model predictions.

METHODS AND MATERIALS

Model of a cytoskeletal polymer attached to a membrane

For simplicity, we begin by considering the conformation of a cytoskeletal polymer on an infinitely large, flat membrane. Without the polymer, the membrane preferentially resides in the x-y plane. The polymer is abstracted as a chain of N monomers, where for convenience N is chosen as odd (for N even, see the Supporting Material), with the middle monomer sitting at the origin, and $(N-1)/2$ monomers on either side along the x axis. Each monomer tightly attaches to the membrane at one point. By assumption the polymer prefers energetically to be curved in the z direction, leading to nonzero membrane height (h) near the polymer, as shown schematically in Fig. 1 *B*. Here we calculate the ground-state conformation of the polymer and the membrane by minimizing the energy of the system.

We assume that the membrane deformation is small in the sense $|\vec{\nabla} h|<<1$, thus the positions of the monomers along the x axis can be accurately approximated as

$$x_j = jd, \tag{1}$$

where

$$j = -j_{\max}, \ldots, j_{\max}, \tag{2}$$

$$N = 2j_{\max} + 1, \tag{3}$$

and where d is the monomer diameter. The heights of the monomers (where the monomers touch the membrane) are $h(x = x_j, y = 0)$. We define the polymer conformation variables h_j as the height of the j^{th} monomer relative to the height of the monomer at the origin:

$$h_j = h\big(x_j, 0\big) - h(0,0). \tag{4}$$

The polymer bending energy, based on elasticity theory (37), is

$$E_p = \frac{B}{2}\int (C - C_0)^2 ds, \tag{5}$$

where B is the polymer bending modulus; C is the local curvature of the polymer; C_0 is the polymer intrinsic curvature; and s is the coordinate along the polymer length. In our model, we write the polymer's local curvature in the discrete form:

$$C_j = \frac{h_{j+1} - 2h_j + h_{j-1}}{d^2}. \tag{6}$$

The bending energy of the discrete polymer can then be expressed as

$$E_p = \frac{Bd}{2}\left[\sum_{j=-j_{\max}+1}^{j_{\max}-1}\left(\frac{h_{j+1} - 2h_j + h_{j-1}}{d^2} - C_0\right)^2\right]. \tag{7}$$

The membrane energy (32,33) can be calculated as the sum of the membrane bending energy and membrane pinning energy, integrated over the entire x-y plane,

$$E_m = \int dxdy\left[\frac{K}{2}\big(\nabla^2 h\big)^2 + \frac{\lambda}{2}h^2\right], \tag{8}$$

where K is the membrane bending modulus, and λ is the membrane pinning modulus. The pinning energy arises from the fact that the turgor pressure inside a cell pushes the cell membrane against the cell wall. The balance between the wall confinement and the turgor pressure defines the ground-state position of the membrane ($h = 0$). Any deviation from this position will result in a pinning energy penalty. We aim to minimize the combined energy,

$$E = E_p + E_m, \tag{9}$$

which will lead to the ground-state membrane and polymer conformation. For simplicity, we initially neglect any intrinsic twist of the polymer. Throughout, we have also neglected any energy contribution from membrane tension because *E. coli* cells with partially lysed cell walls instantly develop large membrane bulges (29,38), indicating an excess of cell membrane and thus little membrane tension in an intact cell.

To minimize the total energy E, we developed a two-step minimization procedure.

First step

We began by calculating the minimized membrane energy E_m for a fixed polymer conformation h_j. Note that the height of the polymer as a whole, denoted by the height of the middle monomer $h(0, 0)$, is also optimized here. To perform this constrained minimization, we introduced multiple Lagrange multipliers (μ_j), and transform the target function into

$$E'_m = E_m - \sum_{j=-j_{\max}}^{j_{\max}} \mu_j h_j. \tag{10}$$

To take advantage of the simple form of E_m in Fourier space, we rewrite the membrane energy and the height constraints as

$$E_m = \frac{1}{2}\int \frac{dq_x dq_y}{(2\pi)^2}\big(Kq^4 + \lambda\big)\tilde{h}_q^2, \tag{11}$$

$$h_j = \int \frac{dq_x dq_y}{(2\pi)^2}\big(e^{iq_x x_j} - 1\big)\tilde{h}_q, \tag{12}$$

where

$$q = \sqrt{q_x^2 + q_y^2}$$

and $\tilde{h}_q$ is the Fourier transform of $h(x, y)$. Solving the equation

$$\frac{\partial E'_m}{\partial \tilde{h}_q} = 0$$

and exploiting the reflection symmetry of the system ($\mu_j = \mu_{-j}$), we obtain

$$\tilde{h}_q = \frac{\sum_{j=1}^{j_{\max}} 2\mu_j\big(\cos q_x x_j - 1\big)}{Kq^4 + \lambda}. \tag{13}$$

This is the membrane conformation in Fourier space with minimized membrane energy. To calculate the values of the Lagrange multipliers, we apply Eq. 13 to the height expression (Eq. 12), and find

$$h_j = \sum_{i=1}^{j_{\max}} \mu_i A_{ij}, \tag{14}$$

where

$$A_{ij} = \int \frac{dq_x dq_y}{(2\pi)^2}\left[\frac{2\big(\cos q_x x_i - 1\big)\big(\cos q_x x_j - 1\big)}{Kq^4 + \lambda}\right]. \tag{15}$$

Defining a matrix A whose elements are A_{ij}, we can write

$$\mu_j = \sum_{i=1}^{j_{\max}} A_{ji}^{-1}\, h_i. \tag{16}$$

We can also apply Eq. 13 to the membrane energy function in Fourier space to obtain

$$E_m = \sum_{j=1}^{j_{\max}}\sum_{i=1}^{j_{\max}} A_{ji}^{-1}\, h_i h_j. \tag{17}$$

Thus, the membrane energy is readily expressed as a function of the polymer conformation.

Second step

In the second step of the minimization, we allow the polymer conformation to vary, and minimize the total energy by solving the following equation:

$$\frac{\partial\left(E_m + E_p\right)}{\partial h_j} = 0, \quad j = 1, \ldots, j_{\max}. \tag{18}$$

As both E_m and E_p are second-order polynomial functions of h_j given by Eqs. 17 and 7, respectively, the derivative gives rise to a set of linear equations that can be readily solved for h_j (see the Supporting Material).

In practice, the only difficulty in numerically solving the above equations stems from the calculation of A_{ij}, which requires a two-dimensional infinite-domain integration. However, by utilizing the following integral definition of a Bessel function,

$$J_0(x) = \frac{1}{\pi}\int_{-\pi/2}^{\pi/2} d\theta \cos(x\cos\theta), \tag{19}$$

we can express A_{ij} as a one-dimensional semiinfinite integral that can be readily numerically evaluated (e.g., by MATLAB, The MathWorks, Natick, MA):

$$A_{ij} = \int_0^\infty dq \frac{q}{\pi(Kq^4+\lambda)}\left[\frac{1}{2}J_0\left(x_i q + x_j q\right) + \frac{1}{2}J_0\left(x_i q - x_j q\right) - J_0(x_i q) - J_0\left(x_j q\right) + 1\right]. \tag{20}$$

A more detailed derivation of the model equations, including the case of N-even, is included in the Supporting Material.

Model parameters

To numerically calculate the polymer and membrane energies and conformations, we employed the following model parameters: The membrane bending modulus was taken from experiment to be 28 kT, where k is the Boltzmann constant, and T is the temperature (300 K) (33–35). As there is no measurement of the membrane pinning modulus λ, we chose the same value 0.28 kT/nm^4 as in Mukhopadhyay et al. (33). For an FtsZ-like polymer, the polymer bending modulus (B) is estimated from the general Young's modulus of globular proteins ($E = 2$ GPa) (39), and the monomer diameter of FtsZ ($d = 4$ nm) (40). Modeling FtsZ as a solid rod, the bending modulus is given by

$$B = \frac{1}{4}\pi\left(\frac{d}{2}\right)^4 E = 6.07 \times 10^3 kT \cdot \text{nm}.$$

Molecular-dynamics simulation of an FtsZ dimer yields a similar estimate (41). A membrane-energy-based model in which FtsZ constricts tubular liposomes through its hydrolysis-independent intermediate curvature also yields an FtsZ bending modulus consistent with our estimate (42). Finally, the intrinsic curvature of the polymer (C_0) was set to be 0.01 nm^{-1} (20).

For an MreB-like polymer, the estimated bending modulus (B) of MreB is 3.79×10^6 $kT\cdot$nm (43). The MreB monomer diameter (d) was measured to be 5.1 nm (13). The preferred orientation of MreB relative to cell circumference (ϕ_0) was measured to be -16° (14). Moreover, the torsional rigidity (τ) of MreB is estimated to be 2.54×10^6 $kT\cdot$nm (43).

The cell radii (R) of *C. crescentus* and *E. coli* are 350 nm and 400 nm, respectively (18,43). The parameters of choice in the calculations are specified in the figure legends.

RESULTS

Long polymers only deform the membrane near their ends

We calculated ground-state polymer and membrane conformations for different polymer lengths. We found that the total energy of the system initially increases slowly with increasing N, then transitions to a steady linear increase by $N \approx 10$ (Fig. 2, *C* and *D*). This energy transition reflects a polymer conformational transition: At smaller N, the whole polymer bends according to its intrinsic curvature; at larger N values, only the ends of the polymer bend in the direction of the intrinsic curvature, with the middle of the polymer actually bending slightly in the opposite direction (Fig. 2, *E–H*). (Note that the scale of the membrane height in the figure is expanded to better present the small deformation, which is at most ~0.2 nm.) As N further increases, the middle of the polymer becomes essentially straight, and approaches $h = 0$ (see Fig. S1 in the Supporting Material). Adding more monomers to the polymer only increases the length of the straight middle section. This is consistent with the observation that the membrane energy approaches a constant value at large N (Fig. 2 *B*), because all of the membrane deformation occurs near the ends of the polymers.

The polymer conformational transition can be intuitively understood by comparing the energy expressions for the polymer (Eq. 5) and the membrane (Eq. 8). If the middle section of a long polymer approaches its intrinsic curvature, rather than being straight, the reduction in the polymer energy is proportional to the length of the section. However, the membrane energy is increased by a higher power of section length because both the area of the deformed membrane (approximately proportional to the length of the middle section) and the extent of the deformation (h) are increased. As a result, for long polymers the middle section adopts a straight conformation and approaches $h = 0$ to minimize the combined energy. To support this explanation, we compared the total energies of the smoothly curved and end-bent conformations using a simplified approximation for these polymer conformations (see Fig. S2, Fig. S3, and Supporting Material for model details). The smoothly curved conformation was approximated as a parabolic function, while the end-bent conformation was approximated as a flat middle section and two parabolic ends. As expected, the smoothly curved conformation is lower in energy for short polymers, but the end-bent conformation becomes lower in energy with increasing polymer length. Intuitively, for long polymers, the membrane-pinning energy prevents large-scale polymer bending and only allows the polymer to bend at the ends where the resulting total membrane height is modest.

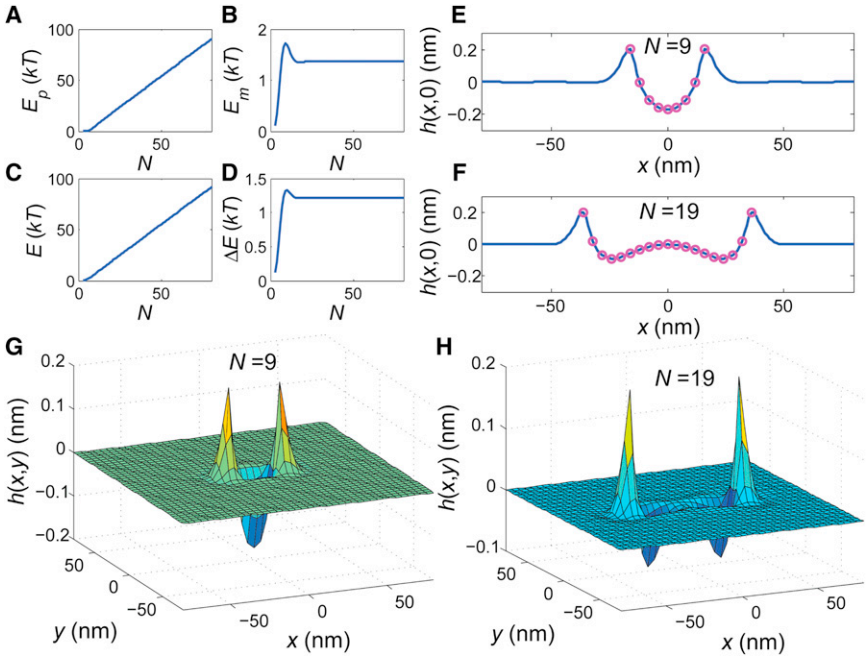

FIGURE 2 Polymer-membrane energies and conformations. (*A–D*) Ground-state polymer bending energy (E_p), membrane energy (E_m), combined energy (E), and energy increment per monomer (ΔE) as functions of polymer length N (energies in units of the thermal energy kT). (*E* and *F*) Membrane and polymer conformations for polymers of length $N = 9$ and 19 oriented along the x axis. (*G* and *H*) Three-dimensional membrane conformations for polymers of length $N = 9$ and 19 from panels *E* and *F*. (Note expanded scale normal to the membrane.) Parameters are: membrane bending modulus $K = 28\ kT$; membrane-pinning modulus $\lambda = 0.28\ kT/\text{nm}^4$; monomer diameter $d = 4$ nm; polymer bending modulus $B = 6.07 \times 10^3\ kT\cdot$ nm; and polymer intrinsic curvature $C_0 = 0.01\ \text{nm}^{-1}$.

Deformation energy sets preferred polymer length

Here, we propose and compare two different mechanisms of polymer length control. For the first mechanism, we assume that the polymer-membrane system has reached equilibrium. In this case, the rates of polymerization and depolymerization reactions are equal. For the second mechanism, we assume that the polymerization reaction is limited by rare nucleation events, i.e., cytoskeletal dimer formation is much less likely than subsequent polymerization. Due to the nucleation limit, there is an excess amount of free monomers waiting for polymerization. In other words, the system is at nonequilibrium.

First mechanism

In the first mechanism, the ground-state polymer length preferred at equilibrium minimizes the total system energy per monomer, which should include the mechanical deformation energy introduced above (E), as well as the monomer-monomer interaction energy (bond enthalpy, ε_{int}). The summed monomer interaction energy in a polymer of length N is $E_{\text{int}} = (N-1)\varepsilon_{\text{int}}$. The total system energy per monomer is therefore

$$\varepsilon_{\text{tot}} = \frac{E + E_{\text{int}}}{N}. \tag{21}$$

In Fig. 3, we plot ε_{tot} as a function of N. Varying the material parameters, we find that the minimum energy usually occurs at $N < 20$ or $N = +\infty$, which means that the preferred filament length is either very short, or maximally long—all available monomers polymerize into one polymer. The lack of intermediate-length polymers is largely attributed to the concave hyperbolic shape of the $(E_{\text{int}})/N$ term in Eq. 21, i.e., the interaction energy per monomer (polymerization benefit) quickly approaches a constant value (ε_{int}) with increasing N, which makes it hard for ε_{tot} to have a global minimum at an intermediate N value. (Note that we have neglected the entropy of the spatial distribution of polymers, which tends to favor shorter filaments.)

Second mechanism

In the nucleation-limited (second) mechanism, the rate of monomer addition at each polymer tip is $k_a[m]$, where k_a is the association rate constant, and $[m]$ is the free monomer concentration; the rate of monomer removal is k_d. The polymerization energy (Gibbs free energy change of the polymerization reaction) can be written as

$$g_{\text{poly}} = -kT \ln\left(\frac{k_a[m]}{k_d}\right), \tag{22}$$

such that negative g_{poly} favors the growth of polymers. On the other hand, polymer elongation is mechanically unfavorable, as it leads to an increase in E. If we define $\Delta E(N) = E(N) - E(N-1)$, the system free-energy increment upon addition of a monomer is

$$\Delta G(N) = \Delta E(N) + g_{\text{poly}}. \tag{23}$$

As a result of the competition between mechanical and chemical energies, the polymer will stop growing when the system free-energy increment ΔG ceases to be negative.

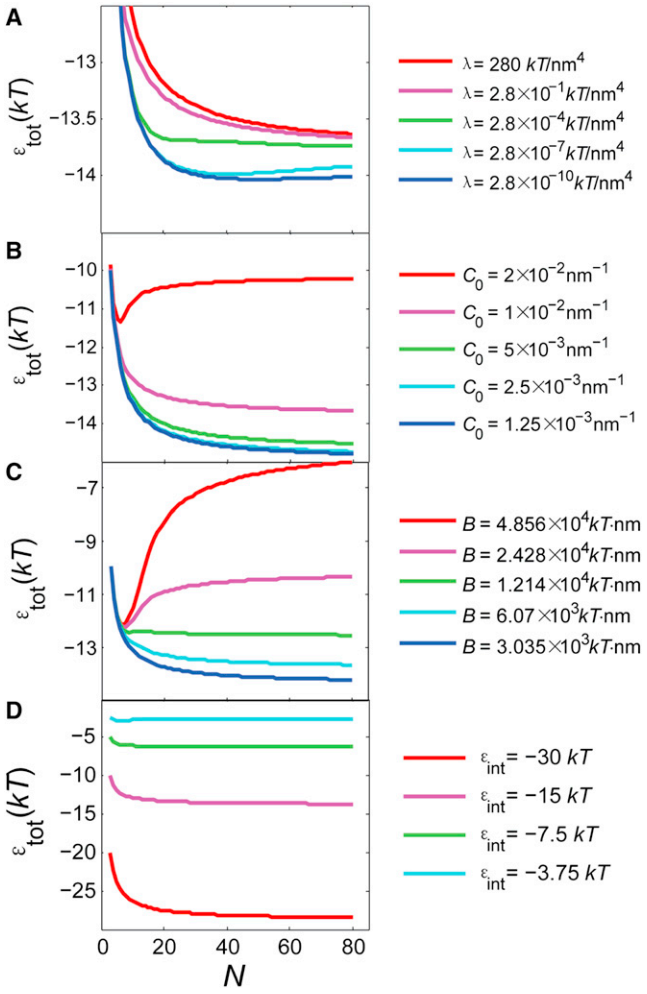

FIGURE 3 Ground-state polymer length. (*A*) Total system energy per monomer ε_{tot} (including monomer-monomer interaction energy ε_{int}) as a function of polymer length N for various pinning moduli. The minimum of each curve is the global ground state. (*B*) ε_{tot} versus N for various polymer intrinsic curvatures. (*C*) ε_{tot} versus N for various polymer bending moduli. (*D*) ε_{tot} versus N for various monomer-monomer interaction energies. Parameters as in Fig. 2 with $\varepsilon_{int} = -15\ kT$, except as indicated.

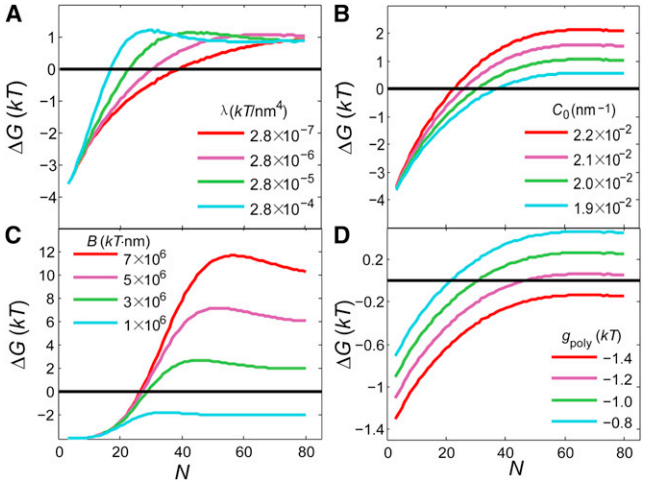

FIGURE 4 Polymer length for nonequilibrium growth conditions. (*A*) System free-energy increment ΔG for monomer addition versus polymer length N for different pinning moduli, with $C_0 = 0.02\ nm^{-1}$. The point of intersection of each energy increment curve with $\Delta G = 0$ (*black line*) indicates where polymer growth stops being energetically favorable. (*B*) ΔG versus N for various intrinsic polymer curvatures, with $\lambda = 2.8 \times 10^{-6}\ kT/nm^4$. (*C*) ΔG versus N for various polymer bending moduli, with $C_0 = 0.001\ nm^{-1}$. (*D*) ΔG versus N for various polymerization energies, with $\lambda = 2.8 \times 10^{-6}\ kT/nm^4$. Parameters as in Fig. 2 with $g_{poly} = -4.0\ kT$, except as indicated.

In Fig. 4, we plot $\Delta G(N)$ versus polymer length N. The value ΔG increases monotonically for small N. The preferred polymer length occurs where the curve intercepts $\Delta G = 0$, such that additional growth is unfavorable. Varying material parameters, we often find moderate preferred lengths with $20 < N < 40$. There are also cases where the $\Delta G(N)$ curve remains below $\Delta G = 0$ (e.g., the *red curve* in Fig. 4 *D*), meaning that polymer will continue to elongate at least until the free monomer concentration is reduced. This divergence of polymer length can happen because the mechanical energy cost of adding monomers $\Delta E(N)$ approaches a constant value after the conformational transition introduced in the previous section. If the constant value is smaller than $|g_{poly}|$, the polymer will favor continuous growth.

When the polymer length is not divergent, the nucleation-limited mechanism favors longer filaments than the equilibrium mechanism does. The reason for this is that the rarity of nucleation events prevents the free monomers from forming many short filaments, even though this configuration is energetically more favorable than fewer, longer filaments.

Our result that membrane mechanics combines with the chemical energy of polymerization to control polymer length may be tested experimentally by quantifying cytoskeletal filament length on a supported lipid membrane in vitro (17). In such an experiment, one may control the monomer chemical potential (concentration), define the membrane composition and pinning, and vary the membrane curvature by forming lipid membrane on substrates patterned with wells or grooves (44). We predict that polymer length will depend not only on the monomer concentration, but also on the mechanical parameters of the membrane and the geometry of the patterns.

In various cytoskeletal systems, NTP-hydrolysis changes the chemical energy of polymerization and thus affects polymer length (45,46). Our model demonstrates that coupled membrane-polymer mechanics can serve as an alternative mechanism of polymer length control, in addition to NTP-hydrolysis dynamics. However, we do not yet know how much each mechanism contributes to the overall distribution of polymer lengths because of

1. Unmeasured parameters in the mechanics model, and
2. Incomplete knowledge of NTP-hydrolysis dynamics in vivo.

In future, the combined effects of hydrolysis and mechanics could prove a fruitful topic for study.

Preferred orientations of FtsZ-like and MreB-like polymers in a rod-shaped cell

Bacterial cytoskeletal filaments usually localize with well-defined cellular orientation. We now ask whether the orientation can be explained by the membrane-polymer energetics introduced in our model. To answer this question, we next calculate the energy of a polymer oriented in various directions on a cylindrical cell membrane. We assume that the membrane bending and pinning energies are still quadratic functions of the deviations from the new ground state (cylindrical membrane), thus our membrane-energy formulation does not need to be changed if one redefines the membrane height (h) as relative to the cylinder, i.e., adopting the Monge representation. The preferred curvature of the polymer in this new coordinate system is the difference between the polymer intrinsic curvature and the curvature of the membrane cylinder in the polymer direction,

$$C_0' = C_0 - C_\phi, \tag{24}$$

with

$$C_\phi = \frac{1}{R}\cos^2\phi, \tag{25}$$

where C_ϕ is the curvature of the membrane cylinder along polymer orientation ϕ (angle relative to circumference of cylinder), and R is the cylinder radius.

We first consider an FtsZ-like polymer, which preferentially localizes in the circumferential direction on a cylindrical membrane. For such a polymer, the intrinsic curvature of the polymer must be bigger than the circumferential curvature of the cell, so that the circumferential direction becomes energetically preferred. Using the original parameters for FtsZ-like polymers except $C_0 = 1/R + 0.01\ \mathrm{nm}^{-1}$, where R is the cell radius of *C. crescentus*, we plot the energy difference for a polymer in the longitudinal versus circumferential direction (Fig. 5 *A*). We find that the energy difference increases dramatically with polymer length. Even a short filament with $20 < N < 40$, as observed in experiment (18), easily distinguishes the longitudinal and circumferential directions. For a polymer with $N = 35$, thermal fluctuation of ~1 kT leads to a polymer orientation fluctuation of <13° (Fig. 5, *B* and *C*).

The model suggests that the elastic and pinning energies resultant from the polymer-membrane interaction ensure the polymer adopts a circumferential orientation with high fidelity. The polymer orientation fluctuation (σ_ϕ) monotonically decreases as a function of polymer length (Fig. 5 *D*), demonstrating that longer polymers orient more accurately. Compared to a rigid membrane as considered in

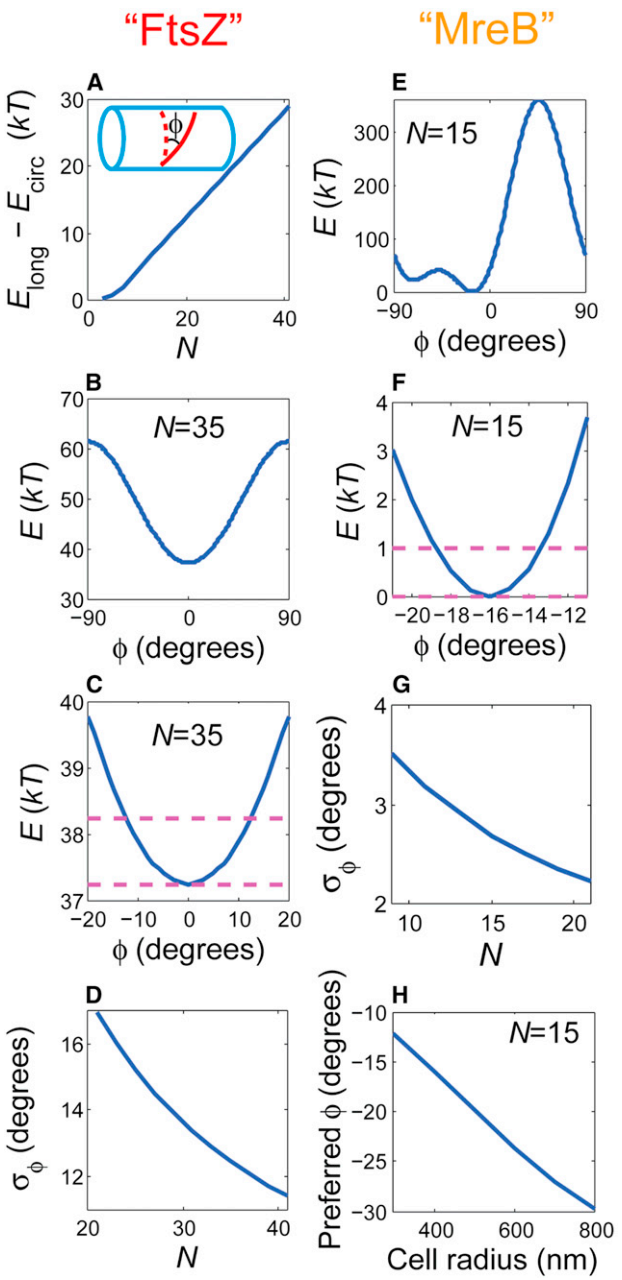

FIGURE 5 Preferred polymer orientation. (*A*) Energy difference between longitudinal ($\phi = 90°$) and circumferential ($\phi = 0°$) orientations as a function of length N for an FtsZ-like polymer, i.e., one with intrinsic curvature bigger than the circumferential curvature of the cell. (*B*) Energy versus FtsZ orientation for $N = 35$. (*C*) Blowup of panel *B*: thermal fluctuation of 1 kT (*magenta lines*) leads to an orientation fluctuation of <13°. (*D*) FtsZ orientation fluctuation (σ_ϕ) versus polymer length. (*E*) Energy versus orientation for an MreB-like polymer, i.e., one with polymer intrinsic curvature less than the circumferential curvature and with a preferred twist. (*F*) Blowup of panel *E*: thermal fluctuation of 1 kT (*magenta lines*) leads to an orientation fluctuation of <3°. (*G*) MreB orientation fluctuation versus polymer length. (*H*) Preferred MreB orientation versus cell radius. Parameters in panels *A–D* are the same as in Fig. 2, except $C_0 = 1/R + 0.01\ \mathrm{nm}^{-1}$, with $R = 350$ nm. Parameters in panels *E–H* are $K = 28\ kT$, $\lambda = 0.28\ kT/\mathrm{nm}^4$, $d = 5.1$ nm, $B = 3.79 \times 10^6\ kT \cdot$ nm, $R = 400$ nm, $C_0 = 2.31 \times 10^{-3}\ \mathrm{nm}^{-1}$, torsional rigidity of the polymer $\tau = 2.54 \times 10^6\ kT \cdot$ nm, and polymer intrinsic twist per unit length $\omega_0 = -6.62 \times 10^{-4}\ \mathrm{nm}^{-1}$.

Andrews and Arkin (36), the inclusion of realistic membrane mechanics leads to a somewhat larger fluctuation in polymer orientation (see Fig. S5). The predicted length dependence of the orientation fluctuation is testable by revisiting electron microscopy experiments on the length and orientation distributions of FtsZ in vivo (18).

To explore other cytoskeletal orientations, we next consider an MreB-like filament, which preferentially localizes in a diagonal/helical direction. A preferred orientation of ϕ_0 implies a polymer intrinsic curvature of

$$C_0 = \frac{1}{R}\cos^2\phi_0, \tag{26}$$

where R is the cell radius of *E. coli*. However, the C_0 values are the same for both ϕ_0 and $-\phi_0$, thus the energy cannot distinguish the left- or right-handed helical conformation of the polymer. To model the chirality of the polymer, we further incorporate an energy contribution from the polymer twist,

$$E_{\text{torsion}} = \frac{1}{2}\tau N d\left[\frac{\sin(2\phi)}{2R} - \omega_0\right]^2, \tag{27}$$

where τ is the torsional rigidity, and the intrinsic twist per unit length ω_0 is set to

$$\omega_0 = \frac{\sin(2\phi_0)}{2R} \tag{28}$$

to also favor the observed orientation angle ϕ_0 in *E. coli*. The new combined energy is

$$E = E_m + E_p + E_{\text{torsion}}. \tag{29}$$

Using measured/estimated parameters for MreB, we show that an MreB-like polymer can also adopt its preferred orientation with high fidelity, even if the polymer is short ($N = 15$) (Fig. 5 *E*). Thermal fluctuation of ~1 kT results in an MreB orientation fluctuation of $<3^\circ$ (Fig. 5 *F*). Again, the orientation fluctuation decreases as the polymer length increases (Fig. 5 *G*), and fluctuations are somewhat larger than for the case of a rigid membrane (36) (see Fig. S5).

Note that in the previous calculation we have been assuming that the intrinsic twist per unit length ω_0 and the intrinsic curvature C_0 of the polymer favors the same polymer orientation ϕ_0. This assumption is not guaranteed to be true, especially when the radius of the cell cylinder is perturbed. If one keeps C_0 and ω_0 constant and increases R, the polymer bending energy favors a smaller ϕ_0, while the torsional energy prefers a bigger ϕ_0, according to Eqs. 26 and 28 (the terms "bigger" and "smaller" here describe the absolute value of ϕ_0). In Fig. 5 *H*, we plot the preferred polymer orientation that minimizes the combined energy at different cylinder radii. For our choice of parameters

$$\omega_0 = \frac{\sin[2 \times (-16^\circ)]}{2 \times 400\ \text{nm}} = -6.62 \times 10^{-4}\text{nm}^{-1}$$

and

$$C_0 = \frac{1}{400\ \text{nm}}\cos^2(-16^\circ) = 2.31 \times 10^{-3}\text{nm}^{-1},$$

the absolute value of the polymer angle increases with R, the direction favored by the polymer torsional energy.

We find that when cylinder radius deviates from the original value (400 nm) where, by assumption, the intrinsic twist per unit length ω_0 and the intrinsic curvature C_0 favor the same polymer orientation, the new preferred polymer angle also depends on polymer length—shorter polymers are more dominated by the torsional energy (see Fig. S4 *A*). This is because short polymers can bend the membrane enough to approach their intrinsic curvature at any orientation. Therefore, for short polymers, there is little orientational dependence of bending energy, and the torsional energy dominates orientation selection. Note that we do not let the membrane deform to accommodate polymer twist, so our theory may not be reliable for very short polymers, in which case membrane deformation may, in reality, significantly lower the torsional energy cost as well. But our theory should capture the tradeoffs for longer polymers, where membrane deformation could not accommodate any substantial polymer twist.

Experimentally, if one can tune cell radius (e.g., by growing cells in rich versus minimal media), and systematically measure the orientations of polymers with different lengths, one may fit the estimated parameters used in the calculations above. Indeed, the preferred polymer angle is sensitive to model parameters λ, C_0, τ, and ω_0 (see Fig. S4 *B*, and *D–F*). The angle is less sensitive to polymer bending modulus B (see Fig. S4 *C*), because the polymer approaches its intrinsic curvature at the choices of B values, and as a result the energy cost of polymer bending hardly varies. However, B can be measured from in vitro force microscopy experiments (47).

Polymer spacing

Bacterial cytoskeleton is sometimes composed of multiple aligned filaments (18). This observation motivates the evaluation of more than one polymer in our model. We ask what spacing of aligned polymers is energetically favorable. To explore the energy landscape, we consider two polymers of the same length either separated far from each other, or perfectly aligned plus in close contact, as shown in Fig. 6 *A*. In the former case, the interaction between the two polymers through membrane deformation can be neglected, and the total energy of the system is twice that of a single polymer on a membrane; in the latter case, the two polymers can be approximated as one polymer with a doubled bending

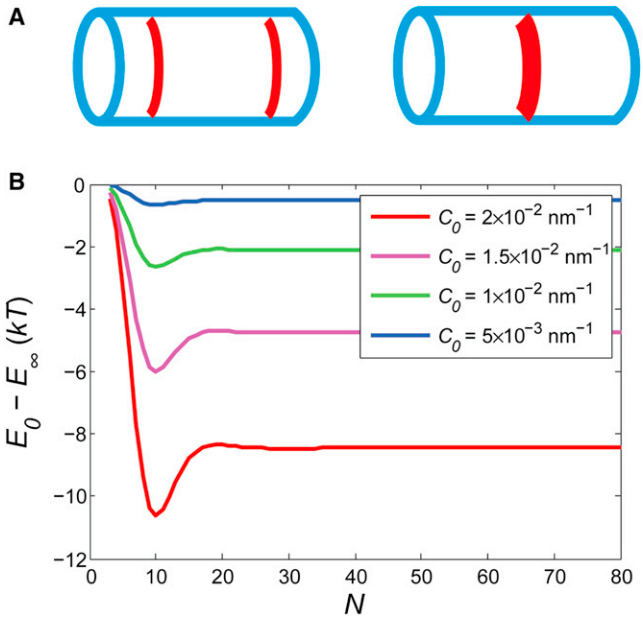

FIGURE 6 Polymer-polymer interaction. (*A*) Schematic illustration of two well-separated FtsZ-like polymers and two adjacent FtsZ-like polymers. (*B*) Energy difference between the two configurations, E_0 for adjacent polymers and E_∞ for well-separated polymers, as a function of polymer length N. Parameters as in Fig. 2, except as indicated.

modulus. In Fig. 6 *B*, we plot the energy difference between these two arrangements as a function of polymer length N. The polymers energetically prefer to be close to each other, rather than widely separated. The energy difference increases with N, peaking for $N = 10$, and saturates at large N. The shape of the function is again related to the conformational transition of the polymers. Before the transition, polymer elongation leads to increased membrane energy E_m (Fig. 2 *B*), suggesting enhanced membrane deformation which strengthens the interaction between adjacent polymers. After the transition, the membrane energy saturates, causing the strength of polymer interaction to saturate. In a previous theoretical work, Shlomovitz and Gov (48) found a similar membrane-mediated attractive interaction between FtsZ rings, under the assumption that both the membrane deformation and the FtsZ density are cylindrically symmetric.

DISCUSSION

We developed a mathematical model for the conformation of a cytoskeletal polymer attached to a bacterial cell membrane, including energetic contributions from polymer bending, membrane bending, and membrane pinning. The model predicts that an intrinsically curved polymer will transit from a smoothly curved conformation to an end-bent conformation with increasing polymer length. Furthermore, the mechanical energy of the polymer-membrane system can regulate polymer length by competing with the favorable chemical energy of polymerization. Importantly, the minimization of mechanical energy can also accurately set the orientations of FtsZ-like and MreB-like polymers on a cylindrical membrane—in a cell-radius-dependent manner—with longer polymers achieving higher accuracy in orientation selection. Finally, polymers on the same membrane mutually attract each other through membrane deformation.

Our prediction of a polymer conformational transition from smoothly curved to end-bent (Fig. 2) is subject to experimental verification through high-resolution microscopy. For our estimated parameters, the membrane deformation is predicted to be ~0.5 nm, which is considerably larger than the resolution limit of state-of-the-art transmission electron microscopy (sub-50 pm) (49). One challenge for such TEM experiments could be that naturally occurring bacterial polymers are too short to observe the predicted transition. This problem may be solved by overexpressing hyperstable mutants of cytoskeletal proteins (e.g., FtsZG109S) (18). In principle, it is also possible to identify mutants with different polymer bending moduli or intrinsic curvatures.

The polymer conformational transition implies that a single cytoskeletal filament has only a limited ability to deform the membrane, because for long polymers most of the membrane remains flat (see Fig. S1). However, filament bundling can increase the combined stiffness of polymers, and thus enhance their ability to deform the membrane. Indeed, in the FtsZ-ring structure, single filaments are bundled laterally (18), which may be necessary to exert biologically meaningful forces on the cell membrane.

Filament bundling can also affect polymer length and orientation. Assuming nucleation-limited polymer assembly, which may typically be the more biologically relevant case, filament bundling will lead to longer polymer lengths. This is because (for example) a bundle of two filaments has twice the favorable polymerization energy, but the combined unfavorable mechanical energy of polymer and membrane deformation is less than doubled (Fig. 6). In addition, stiffer bundles imply orientation selection with higher fidelity, because deviations from the preferred orientation will now result in a stronger penalty in polymer-bending/twisting energy. Importantly, in order for the bundle to maintain the intrinsic curvature of a single filament and correctly attach to the membrane, individual filaments in the bundle must have a coherent orientation of their membrane binding domain (i.e., each filament must expose the same face of monomers to the membrane).

Besides bundling with each other, cytoskeletal polymers can also be associated with auxiliary proteins, which may serve as membrane anchors. For example, FtsZ is indirectly tethered to the cell membrane by FtsA and ZipA (10). Although for simplicity our model assumed direct attachment of polymers to the membrane, the presence of auxiliary attachment proteins does not change the model

derivation, and thus the general conclusions remain valid. On the other hand, certain auxiliary proteins may be sandwiched between adjacent cytoskeletal filaments in a bundle, and set the minimum distance between filaments. This may explain why the spacing of FtsZ filaments in vivo (~9.3 nm) (18) is larger than the diameter of FtsZ monomers (4 nm) (18), even though our model predicts an attraction between parallel filaments through membrane deformation.

Another simplification in the model is that the polymer intrinsic curvature is assumed to be homogeneous. However, using the same mathematical framework, one can readily solve for the conformation of a membrane-associated nonhomogenous polymer, i.e., with the intrinsic curvature C_0 in Eq. 7 no longer constant along the polymer. Such a modification could be relevant to the analysis of partially hydrolyzed FtsZ polymers, including polymers formed of both wild-type and nonhydrolyzing-mutant monomers. If hydrolysis rates depend on local strain in the polymer, then polymer inhomogeneity could both affect and be affected by the membrane-polymer conformation.

On the cell membrane, a growing FtsZ filament may start to undergo internal GTP hydrolysis before reaching its preferred length. The resultant increase in intrinsic curvature can reduce the preferred length, and once the preferred length is reduced to the current length, the filament will naturally transit from growth to shrinkage. A similar dynamic-instability scenario for substrate-absorbed cytoskeletal polymers has been proposed by Zapperi and Mahadevan (50).

During cell division, a cell constricts at the middle, where FtsZ is localized (10). Such a decrease in cell diameter may affect the FtsZ polymer conformation. In our model, a decrease in cell diameter leads to a reduction of the bending energy of an FtsZ-like polymer (Eq. 24). As a result, the polymer length may increase (Fig. 4). In addition, the energy difference between well-separated and closely packed polymers becomes smaller (Fig. 6), which suggests that the polymers may become less tightly spaced as constriction proceeds.

Our result that the orientation of MreB-like polymers depends on cell radius implies a potential feedback mechanism for cell-width control. A previous computational work showed that a more diagonal (less circumferential) MreB orientation leads to a more diagonal glycan strand insertion direction (with the opposite chirality) in the cell wall (14), which then results in an increase in cell radius (51). On the other hand, our analysis suggests that in response to an increase in cell radius, MreB could adopt either a more or less circumferential orientation depending on physical parameters (see Fig. S4). If MreB prefers a more circumferential orientation with increasing cell radius (i.e., polymer bending energy dominates orientation selection), this change in MreB orientation will negatively feed-back onto the cell radius (14,51), providing a homeostatic mechanism. To evaluate this potential feedback mechanism, MreB orientation could be measured in cells or vesicles of controlled shapes (52,53), and the relevant physical parameters measured in vitro.

Although we have only analyzed the orientation selection of MreB- and FtsZ-like polymers, both of which prefer concave curvatures, our model applies to polymers with convex curvatures as well. For example, CreS localizes along the inner, convex curvature of *C. crescentus* cells (9). If CreS filaments have a convex intrinsic curvature, both the localization and orientation of CreS filaments may be explained by minimization of the mechanical energy of the system.

Polymer-polymer interaction through membrane deformation provides a self-assembly mechanism that can facilitate the formation of cytoskeletal structures, such as bundles and sheets. Recently, FtsZ in several bacterial species has been imaged with superresolution microscopy, in all cases revealing a bundled FtsZ conformation (54–57). Interestingly, our observation that long polymers deform the membrane only near their ends implies that membrane-mediated attractive interactions will occur between the ends of such polymers. Similarly, interactions of long polymers with other structures that deform the membrane, e.g., curved lipid rafts and membrane bending proteins, will also occur at the polymer end, and can be attractive or repulsive depending on the induced membrane curvature.

Previous works have modeled the localization and interaction of intrinsically curved lipid rafts on a cell membrane (32,33). Given the insights we gained from this work, we predict that two-dimensional lipid rafts with intrinsic curvature might also undergo a conformational transition similar to that of the one-dimensional cytoskeletal polymer, if the rafts can grow big enough and the membrane-pinning modulus is not zero. Intuitively, a raft with a uniform curvature and diameter L will lead to a membrane height $\sim L^2$ and thus a total membrane energy $\sim L^6$ (L^2 from the area and L^4 from the pinning-energy density). In contrast, a flat raft will have an energy $\sim L^2$ due to the curvature mismatch integrated over the raft's area. Thus, at a certain raft size the uniformly curved conformation will no longer be energetically favorable, and the central region of the raft will start to approach zero membrane height to lower the pinning energy. Nevertheless, it is possible that a raft can never reach this critical size because smaller, separate rafts are more energetically favorable. These considerations can certainly limit the growth of lipid domains (32,33).

Recently the focus of synthetic biology has begun to turn from gene regulation toward engineered cellular structures. Our findings can serve as a guide for engineering novel cytoskeletal proteins with specific cellular orientations. Because mechanical energy can dictate the orientation of cytoskeleton, we only need to make the synthetic polymer:

1. Intrinsically curved and/or twisted to the desired extent;
2. Comparable in length and stiffness to naturally occurring cytoskeletal filaments; and

3. Able to bind to cell membrane with the correct face of the polymer.

We look forward to the experimental realization of such ideas.

SUPPORTING MATERIAL

Five figures are available at http://www.biophysj.org/biophysj/supplemental/S0006-3495(12)05140-5.

We acknowledge valuable conversations with Zemer Gitai, Chris Henley, K. C. Huang, Joshua Shaevitz, and Sven van Teeffelen.

This work was supported in part by National Institutes of Health grant No. R01 GM073186 and in part by National Science Foundation grant No. PHY-0957573.

REFERENCES

1. Young, K. D. 2006. The selective value of bacterial shape. *Microbiol. Mol. Biol. Rev.* 70:660–703.
2. Dusenbery, D. B. 1998. Fitness landscapes for effects of shape on chemotaxis and other behaviors of bacteria. *J. Bacteriol.* 180:5978–5983.
3. Cooper, S., and M. W. Denny. 1997. A conjecture on the relationship of bacterial shape to motility in rod-shaped bacteria. *FEMS Microbiol. Lett.* 148:227–231.
4. Cho, H., H. Jönsson, …, A. Levchenko. 2007. Self-organization in high-density bacterial colonies: efficient crowd control. *PLoS Biol.* 5:e302.
5. Cabeen, M. T., and C. Jacobs-Wagner. 2005. Bacterial cell shape. *Nat. Rev. Microbiol.* 3:601–610.
6. Gitai, Z. 2005. The new bacterial cell biology: moving parts and subcellular architecture. *Cell.* 120:577–586.
7. Gitai, Z., N. A. Dye, …, L. Shapiro. 2005. MreB actin-mediated segregation of a specific region of a bacterial chromosome. *Cell.* 120: 329–341.
8. Karczmarek, A., R. Martínez-Arteaga, …, T. den Blaauwen. 2007. DNA and origin region segregation are not affected by the transition from rod to sphere after inhibition of *Escherichia coli* MreB by A22. *Mol. Microbiol.* 65:51–63.
9. Ausmees, N., J. R. Kuhn, and C. Jacobs-Wagner. 2003. The bacterial cytoskeleton: an intermediate filament-like function in cell shape. *Cell.* 115:705–713.
10. Adams, D. W., and J. Errington. 2009. Bacterial cell division: assembly, maintenance and disassembly of the Z ring. *Nat. Rev. Microbiol.* 7:642–653.
11. Errington, J., R. A. Daniel, and D. J. Scheffers. 2003. Cytokinesis in bacteria. *Microbiol. Mol. Biol. Rev.* 67:52–65.
12. Vats, P., and L. Rothfield. 2007. Duplication and segregation of the actin (MreB) cytoskeleton during the prokaryotic cell cycle. *Proc. Natl. Acad. Sci. USA.* 104:17795–17800.
13. van den Ent, F., L. A. Amos, and J. Löwe. 2001. Prokaryotic origin of the actin cytoskeleton. *Nature.* 413:39–44.
14. Wang, S., L. Furchtgott, …, J. W. Shaevitz. 2012. Helical insertion of peptidoglycan produces chiral ordering of the bacterial cell wall. *Proc. Natl. Acad. Sci. USA.* 109:E595–E604.
15. Bendezú, F. O., and P. A. de Boer. 2008. Conditional lethality, division defects, membrane involution, and endocytosis in MRE and MRD shape mutants of *Escherichia coli*. *J. Bacteriol.* 190:1792–1811.
16. Cabeen, M. T., G. Charbon, …, C. Jacobs-Wagner. 2009. Bacterial cell curvature through mechanical control of cell growth. *EMBO J.* 28:1208–1219.
17. Salje, J., F. van den Ent, …, J. Löwe. 2011. Direct membrane binding by bacterial actin MreB. *Mol. Cell.* 43:478–487.
18. Li, Z., M. J. Trimble, …, G. J. Jensen. 2007. The structure of FtsZ filaments in vivo suggests a force-generating role in cell division. *EMBO J.* 26:4694–4708.
19. Lu, C., M. Reedy, and H. P. Erickson. 2000. Straight and curved conformations of FtsZ are regulated by GTP hydrolysis. *J. Bacteriol.* 182:164–170.
20. Mingorance, J., M. Tadros, …, M. Vélez. 2005. Visualization of single *Escherichia coli* FtsZ filament dynamics with atomic force microscopy. *J. Biol. Chem.* 280:20909–20914.
21. Osawa, M., D. E. Anderson, and H. P. Erickson. 2008. Reconstitution of contractile FtsZ rings in liposomes. *Science.* 320:792–794.
22. Allard, J. F., and E. N. Cytrynbaum. 2009. Force generation by a dynamic Z-ring in *Escherichia coli* cell division. *Proc. Natl. Acad. Sci. USA.* 106:145–150.
23. Lan, G., A. Dajkovic, …, S. X. Sun. 2008. Polymerization and bundling kinetics of FtsZ filaments. *Biophys. J.* 95:4045–4056.
24. Lan, G., B. R. Daniels, …, S. X. Sun. 2009. Condensation of FtsZ filaments can drive bacterial cell division. *Proc. Natl. Acad. Sci. USA.* 106:121–126.
25. Erickson, H. P. 2009. Modeling the physics of FtsZ assembly and force generation. *Proc. Natl. Acad. Sci. USA.* 106:9238–9243.
26. Ghosh, B., and A. Sain. 2008. Origin of contractile force during cell division of bacteria. *Phys. Rev. Lett.* 101:178101.
27. Fischer-Friedrich, E., and N. Gov. 2011. Modeling FtsZ ring formation in the bacterial cell-anisotropic aggregation via mutual interactions of polymer rods. *Phys. Biol.* 8:026007.
28. Paez, A., P. Mateos-Gil, …, P. Tarazona. 2009. Simple modeling of FtsZ polymers on flat and curved surfaces: correlation with experimental in vitro observations. *PMC Biophys.* 2:8.
29. Deng, Y., M. Z. Sun, and J. W. Shaevitz. 2011. Direct measurement of cell wall stress stiffening and turgor pressure in live bacterial cells. *Phys. Rev. Lett.* 107:158101.
30. Cayley, S., B. A. Lewis, …, M. T. Record, Jr. 1991. Characterization of the cytoplasm of *Escherichia coli* K-12 as a function of external osmolarity. Implications for protein-DNA interactions in vivo. *J. Mol. Biol.* 222:281–300.
31. Wood, J. M. 2007. Bacterial osmosensing transporters. *Methods Enzymol.* 428:77–107.
32. Huang, K. C., R. Mukhopadhyay, and N. S. Wingreen. 2006. A curvature-mediated mechanism for localization of lipids to bacterial poles. *PLOS Comput. Biol.* 2:e151.
33. Mukhopadhyay, R., K. C. Huang, and N. S. Wingreen. 2008. Lipid localization in bacterial cells through curvature-mediated microphase separation. *Biophys. J.* 95:1034–1049.
34. Wiggins, P., and R. Phillips. 2005. Membrane-protein interactions in mechanosensitive channels. *Biophys. J.* 88:880–902.
35. Rawicz, W., K. C. Olbrich, …, E. Evans. 2000. Effect of chain length and unsaturation on elasticity of lipid bilayers. *Biophys. J.* 79:328–339.
36. Andrews, S. S., and A. P. Arkin. 2007. A mechanical explanation for cytoskeletal rings and helices in bacteria. *Biophys. J.* 93:1872–1884.
37. Landau, L. D., E. M. Lifshitz, …, E. H. Dill. 1960. Theory of elasticity: Vol. 7. of Course of Theoretical Physics. *Phys. Today.* 13:44.
38. Huang, K. C., R. Mukhopadhyay, …, N. S. Wingreen. 2008. Cell shape and cell-wall organization in Gram-negative bacteria. *Proc. Natl. Acad. Sci. USA.* 105:19282–19287.
39. Kojima, H., A. Ishijima, and T. Yanagida. 1994. Direct measurement of stiffness of single actin filaments with and without tropomyosin by in vitro nanomanipulation. *Proc. Natl. Acad. Sci. USA.* 91:12962–12966.
40. Erickson, H. P., D. W. Taylor, …, D. Bramhill. 1996. Bacterial cell division protein FtsZ assembles into protofilament sheets and mini-rings, structural homologs of tubulin polymers. *Proc. Natl. Acad. Sci. USA.* 93:519–523.

41. Hsin, J., A. Gopinathan, and K. C. Huang. 2012. Nucleotide-dependent conformations of FtsZ dimers and force generation observed through molecular dynamics simulations. *Proc. Natl. Acad. Sci. USA.* 109: 9432–9437.

42. Cytrynbaum, E. N., Y. D. Li, …, H. Mehrabian. 2012. Estimating the bending modulus of a FtsZ bacterial-division protein filament. *Phys. Rev. E Stat. Nonlin. Soft Matter Phys.* 85:011902.

43. Wang, S., H. Arellano-Santoyo, …, J. W. Shaevitz. 2010. Actin-like cytoskeleton filaments contribute to cell mechanics in bacteria. *Proc. Natl. Acad. Sci. USA.* 107:9182–9185.

44. Steltenkamp, S., M. M. Müller, …, A. Janshoff. 2006. Mechanical properties of pore-spanning lipid bilayers probed by atomic force microscopy. *Biophys. J.* 91:217–226.

45. Bean, G. J., and K. J. Amann. 2008. Polymerization properties of the *Thermotoga maritima* actin MreB: roles of temperature, nucleotides, and ions. *Biochemistry.* 47:826–835.

46. Chen, Y., and H. P. Erickson. 2005. Rapid in vitro assembly dynamics and subunit turnover of FtsZ demonstrated by fluorescence resonance energy transfer. *J. Biol. Chem.* 280:22549–22554.

47. Dupuis, D. E., W. H. Guilford, …, D. M. Warshaw. 1997. Actin filament mechanics in the laser trap. *J. Muscle Res. Cell Motil.* 18:17–30.

48. Shlomovitz, R., and N. S. Gov. 2009. Membrane-mediated interactions drive the condensation and coalescence of FtsZ rings. *Phys. Biol.* 6:046017.

49. Erni, R., M. D. Rossell, …, U. Dahmen. 2009. Atomic-resolution imaging with a sub-50-pM electron probe. *Phys. Rev. Lett.* 102:096101.

50. Zapperi, S., and L. Mahadevan. 2011. Dynamic instability of a growing adsorbed polymorphic filament. *Biophys. J.* 101:267–275.

51. Furchtgott, L., N. S. Wingreen, and K. C. Huang. 2011. Mechanisms for maintaining cell shape in rod-shaped Gram-negative bacteria. *Mol. Microbiol.* 81:340–353.

52. Renner, L. D., and D. B. Weibel. 2011. Cardiolipin microdomains localize to negatively curved regions of *Escherichia coli* membranes. *Proc. Natl. Acad. Sci. USA.* 108:6264–6269.

53. Männik, J., R. Driessen, …, C. Dekker. 2009. Bacterial growth and motility in sub-micron constrictions. *Proc. Natl. Acad. Sci. USA.* 106:14861–14866.

54. Fu, G., T. Huang, …, J. Xiao. 2010. In vivo structure of the E. coli FtsZ-ring revealed by photoactivated localization microscopy (PALM). *PLoS ONE.* 5:e12682.

55. Jennings, P. C., G. C. Cox, …, E. J. Harry. 2010. Super-resolution imaging of the bacterial cytokinetic protein FtsZ. *Micron.* 42:336–341.

56. Biteen, J. S., E. D. Goley, …, W. E. Moerner. 2012. Three-dimensional super-resolution imaging of the midplane protein FtsZ in live *Caulobacter crescentus* cells using astigmatism. *Chem. Phys. Chem.* 13:1007–1012.

57. Strauss, M. P., A. T. Liew, …, E. J. Harry. 2012. 3D-SIM super resolution microscopy reveals a bead-like arrangement for FtsZ and the division machinery: implications for triggering cytokinesis. *PLoS Biol.* 10:e1001389.